J. Fluid Mech. (1983), *vol.* 128, *pp.* 323–346
Printed in Great Britain

The effect of a passive cross-stream temperature gradient on the evolution of temperature variance and heat flux in grid turbulence

By A. SIRIVAT† AND Z. WARHAFT

Sibley School of Mechanical and Aerospace Engineering, Cornell University, Ithaca, NY 14853

(Received 15 January 1982 and in revised form 4 October 1982)

The evolution of temperature variance and heat flux in decaying grid turbulence with a linear cross-stream temperature gradient is studied by producing the temperature gradient by means of two different methods: (*a*) by placing a 'mandoline' (Warhaft & Lumley 1978) downstream from the grid but with its wires differentially heated for the present study, and (*b*) by differentially heating ribbons of nichrome (a 'toaster') placed in the plenum chamber of the wind tunnel. For the former method the initial thermal/mechanical lengthscale ratio L_θ/L was varied by changing the mandoline configuration. For this method it is shown that the gradient causes L_θ/L to equilibrate to a value of about 0·9 regardless of its initial value, and that when this value is achieved the temperature variance increases approximately linearly with time. The toaster was used to produce a temperature gradient without the associated initial temperature variance (and initial thermal lengthscale) that is necessarily produced by the mandoline wires; for the toaster the temperature variance was produced solely by the action of turbulence against the temperature gradient. For this experiment too, the thermal variance grew linearly with time, and L_θ/L was approximately the same as the equilibrium value for the mandoline experiments. The equilibrium value of the ratio of temperature-variance production to temperature-variance dissipation was approximately 1·5 for all of the experiments. The ratio of the mechanical-dissipation/thermal-dissipation timescales was also found to equilibrate, but there was considerably more scatter in the data for this parameter. The values of the equilibrium length- and timescale ratios were not affected by the magnitude of the temperature gradient, which was varied for both experiments. Good transverse homogeneity in the thermal field was achieved in all cases, in contrast with previous experiments (using heated grids).

1. Introduction

Corrsin (1952) predicted for non-decaying isotropic turbulence flowing with a mean velocity U in the x-direction that an imposed passive linear cross-stream temperature gradient dT/dz (from here on denoted as β) will maintain itself, and is independent of x. The reason for this is that at any point in this flow there is equal probability of a particle arriving at that point with a deficit or an excess of temperature. Thus the mean temperature along a mean streamline will not change. Although Corrsin only considered a stationary non-decaying (non-evolving) flow, his prediction for the constancy of β has had remarkable confirmation for decaying grid turbulence in which the temperature gradient was produced by differentially heating the bars of

† Present address: Department of Chemical Engineering, The Johns Hopkins University, Baltimore, Maryland 21218.

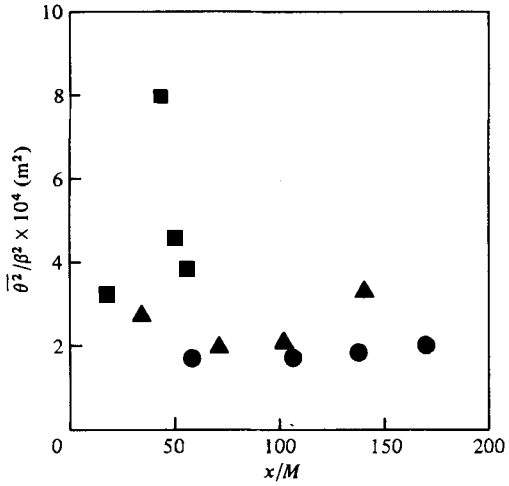

FIGURE 1. Evolution of $\overline{\theta^2}/\beta^2$ from previous experiments: ▲, Wiskind (1962); ●, Alexopoulos & Keffer (1971); ■, Venkataramani & Chevray (1978). The values have been obtained by averaging over the core of the flows.

the grid (Wiskind, 1962; Alexopoulos & Keffer 1971; Venkataramani & Chevray 1978). In all of these experiments β = constant and its value was independent of x.

However, the streamwise evolution of the temperature variance $\overline{\theta^2}$ and the gradient (cross-stream) heat flux $\overline{\theta w}$ in these flows is poorly understood from both experimental and theoretical viewpoints.

Figure 1 shows $\overline{\theta^2}/\beta^2$ as a function of x/M, where M is the grid mesh length, for the three experiments cited above.† It is not clear from these experiments whether $\overline{\theta^2}$ increases or decreases with x/M: Wiskind (1962) and Alexopoulos & Keffer (1971) both show an increase (after about $x/M = 50$) but the rates are different; Venkataramani & Chevray (1978) show a dramatic increase followed by an equally dramatic decrease, but their experiment only extends to $x/M \approx 50$. Part of the reason for the large scatter in these data probably lies in the method of generating the thermal profile: in all cases it was generated by heating the bars of the grid. Heating the grid bars differentially not only produces a temperature gradient; it also produces a cross-stream gradient in $\overline{\theta^2}$ since, the hotter the bar, the greater temperature variance produced in its wake. Figure 2 shows the r.m.s. θ cross-stream profiles for the above-cited experiments. Cross-stream variations of r.m.s. θ of 30–40 % occur in only few mesh lengths, a situation far from ideal, which is for no variation of $\overline{\theta^2}$ in the cross-stream direction but only for a mean gradient β. Furthermore, as has been shown by Warhaft & Lumley (1978), heating a grid also produces significant longitudinal heat flux, and this coupling of the velocity and temperature fluctuations probably also affects the evolution of $\overline{\theta^2}$. Ideally there should be no coupling between the temperature fluctuations and the longitudinal velocity in such an experiment; the only flux should be down the temperature gradient, i.e. in the cross-stream direction.

From a theoretical viewpoint, the evolution of $\overline{\theta^2}$ has been examined using classical dispersion theory. For a linear temperature gradient in decaying turbulence, but without the action of thermal dissipation, Sullivan (1976) finds that $\overline{\theta^2}$ should increase

† We have determined $\overline{\theta^2}/\beta^2$ by averaging $\overline{\theta^2}$ across the core of the flows for these experiments. Sullivan (1976) finds a faster rate of increase of $\overline{\theta^2}/\beta^2$ for the Alexopoulos & Keffer (1971) experiment by excluding from his averaging procedure values of $\overline{\theta^2}$ that initially decline with distance.

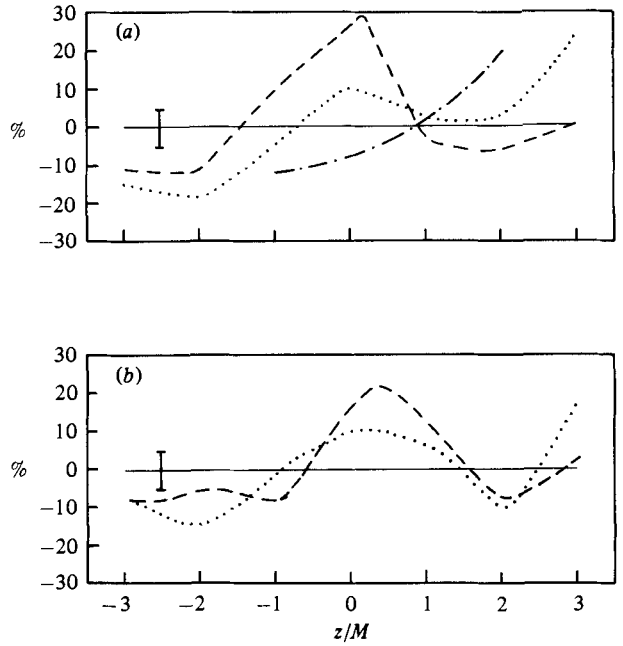

FIGURE 2. Departure of r.m.s. θ from its mean level in the cross-stream direction. (*a*) ---, Wiskind, $x/M = 71$; · · ·, Alexopoulos & Keffer, $x/M = 60$; —·—·, Venkataramani & Chevray, $x/M = 55$. (*b*) Wiskind, $x/M = 102$; Alexopoulos & Keffer, $x/M = 108$; same symbols as for (*a*). The vertical bars show the maximum r.m.s. θ-deviation (at $x/M = 80$ (*a*) and $x/M = 110$ (*b*)) for the results to be presented in 3.2.

linearly with time, i.e. $\overline{\theta^2}/\beta^2 \propto t$. More recently Durbin (1980) has examined this problem using two-particle dispersion theory which includes the effects of dissipation and he finds that $\overline{\theta^2}/\beta^2 \propto t^{0.5}$.†

It is instructive to examine the conservation equations for $\overline{\theta^2}$ and $\overline{\theta w}$. Assuming transverse homogeneity the equations are (Tennekes & Lumley 1972):

$$\frac{1}{2}\frac{d\overline{\theta^2}}{dt} = -\overline{\theta w}\beta - \epsilon_\theta, \tag{1}$$

$$\frac{d\overline{\theta w}}{dt} = -\overline{w^2}\beta - \frac{1}{\rho_0}\overline{\theta\frac{\partial p}{\partial z}}. \tag{2}$$

Here ϵ_θ is the temperature-dissipation term, p is the pressure fluctuation and ρ_0 is a reference density. Other terms have been defined above. Note that, since the gradient is passive, no buoyancy term appears in (2). Equation (1) shows that there is both production and dissipation of $\overline{\theta^2}$, and in order to model $\overline{\theta^2}(t)$ it is necessary to have an understanding of how the gradient production affects the thermal-variance dissipation. It should be noted that even for the apparently simple case for which $\beta = 0$ (the decay of thermal fluctuations) we still have not resolved the question of the equilibrium $\overline{\theta^2}$ decay rate (Warhaft & Lumley 1978). Equation (2) for $\overline{\theta w}$ also has a production term, but the dissipation of $\overline{\theta w}$ is negligible in these flows of

† We note that in these analyses Sullivan (1976) assumes that the Reynolds number of the decaying flow is constant, while Durbin (1980) assumes the turbulence is non-decaying. For the decaying turbulence realized in the laboratory the turbulence Reynolds number decreases as t^{1-n}, where $n \approx 1{\cdot}3$.

moderately high Re and has been neglected; the destruction of $\overline{\theta w}$ is effected by the temperature–pressure fluctuation-gradient product; the return to isotropy term.

For a stationary flow with a non-evolving heat flux, and assuming the thermal variance dissipation to be zero, (1) yields $\overline{\theta^2} \propto t$, but if, as is the case in grid turbulence, the flow is evolving and there is dissipation, assumptions must be made concerning the velocity field and the dissipation mechanisms. For example, if for the velocity variance we use the empirical relation $\overline{u^2} \propto t^{-n}$, where $n \approx 1{\cdot}3$ for decaying grid turbulence, and if we assume the eddy diffusivity K_θ ($\equiv -\overline{\theta w}/\beta$) is proportional to ul, where l is the integral scale of the turbulence, then $K_\theta \propto t^{1-n}$. Further, if we assume that the mechanical to thermal timescale ratio is unity then we may write $\epsilon_\theta = \overline{\theta^2}/\tau$, where τ is the mechanical timescale ($\equiv 3\overline{u^2}/\epsilon$). Substituting these expressions for K_θ and ϵ_θ into (1) yields that $\overline{\theta^2}$ is approximately proportional to $t^{2-n} = t^{0{\cdot}7}$, i.e. the thermal variance grows at a less-than-linear rate. However, this crude analysis relies on simple eddy-diffusivity concepts, and, furthermore, it cannot predict the effect of varying the mechanical/thermal timescale ratio on the evolution of $\overline{\theta^2}$, one of the primary concerns of this study. Nevertheless it is clear that both dispersion theory and a rudimentary examination of the conservation equations suggest an increase of $\overline{\theta^2}$ with time. There is, though, no agreement on the actual rate of increase of $\overline{\theta^2}$, and the available experimental data (figure 1) shed little light on this question.

Our objective here, then, is to experimentally examine the evolution $\overline{\theta^2}$ and $\overline{\theta w}$ in decaying grid turbulence with a mean cross-stream temperature gradient. In order to avoid the problems of cross-stream inhomogeneity, we will use two new methods for the production of the temperature gradient. We will also pay particular attention to varying input conditions such as the strength of the temperature gradient, the initial thermal scale and the mean tunnel speed.

2. Apparatus and method of approach

The open-circuit vertical wind tunnel (figure 3) was the same as that used in our previous studies (Warhaft 1980). The mesh length M of the biplane turbulence-generating grid was 0·025 m and the grid bars were 0·476 cm square-sectioned, giving a grid solidity of 0·34. The tunnel test section was $200M$ long and $16M \times 16M$ in cross-section. The walls of the tunnel were slightly divergent to ensure a constant centreline mean speed with the development of the boundary layer. The mean wind speed was 3·4 m/s for most of the mandoline experiments and 6·3 m/s for the toaster experiments (see below).

The temperature profiles were produced by two different methods. For the first method a 'mandoline' (Warhaft & Lumley 1978), a parallel array of fine wires, was placed downstream from the grid and the wires were differentially heated. This was achieved by independently controlling the voltage (and hence current) across each wire. Because of the change in resistance with wire heating and because of wall effects, 'fine tuning' of the current in each wire was needed in order to achieve linear temperature gradients, which were varied from 1·81 °C/m to 8·1 °C/m, for the different experiments to be described below. The actual values of the currents used are reported in Sirivat (1983). The mandoline wires were $1{\cdot}27 \times 10^{-4}$ m diameter (and for a few experiments $2{\cdot}03 \times 10^{-4}$ m diameter), giving cold-flow Reynolds numbers of 26 (and sometimes 42) for the low speeds (3·4 m/s) at which most of the mandoline experiments were carried out. It should be noted that when the wires are heated the Reynolds number is reduced well below the vortex-shedding Re of approximately 40 since the viscosity of the surrounding air increases considerably.

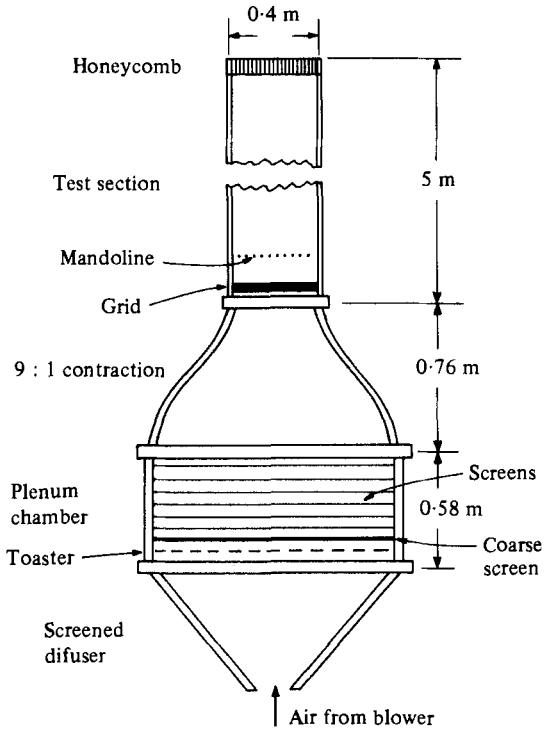

FIGURE 3. The wind tunnel showing the mandoline and toaster.

As explained in §1, the previous gradient experiments all used differentially heated grid bars. This method of producing the temperature gradient also produces an initial temperature variance, a complicating condition since ideally all the temperature variance should be created by production against the gradient. When designing the present experiment we realized that the same situation would apply to the mandoline: it too would produce initial temperature variance as well as the gradient.† Thus we sought a different method, one that would produce a linear gradient only. For this second method we produced the temperature gradient deep down in the plenum chamber (figure 3) by differentially heating nicrome ribbons placed in a parallel array. As for the mandoline, this was achieved by independently controlling the current in each ribbon. The values of the current in each ribbon are reported in Sirivat (1983). The ribbons were 3·175 mm wide and 0·101 mm thick and were placed in pairs (giving an effective width of about 7 mm). Sixteen pairs of these ribbons equally spaced in the plenum chamber were used to form a 'toaster', so named because of its resemblance to the elements in the kitchen appliance of the same name.‡ The

† However, as will be shown in §3, the mandoline produces a far more homogeneous temperature field than the heated grid experiments. Furthermore, by means of the mandoline we were able to vary the input thermal scale and study its evolution in the presence of the temperature gradient (which imposes its own lengthscale). This type of experiment can only be done if there is an initial temperature variance, with its own scale, that is different to that produced by the gradient. For this type of experiment the mandoline is ideally suited.

‡ To be consistent with our use of the word *mandoline* (named after the French kitchen utensil used to chop and slice vegetables (Warhaft & Lumley 1978)) it might have been more appropriate to use the French term *grille-pain* instead of toaster. In this instance the English word seemed less cumbersome.

rationale for creating the gradient in the plenum was that any disturbance to the flow produced by the nicrome ribbons would be damped out by the screens and the contraction (figure 3), and by the time the flow reached the grid a linear temperature gradient (in laminar flow) would only be present. Any temperature fluctuations subsequently produced would be solely due to the action of the grid turbulence against the temperature gradient.

In order to produce a linear gradient rather than a series of hot blips above the toaster elements, we placed a very coarse screen of sheet metal, with a lattice of 6·5 mm circular holes and a solidity of 0·46, downstream of the toaster to cause turbulent mixing. This was only partially effective; there were blips in the mean temperature profile measured in the test section without the grid in the flow (but the r.m.s. temperature and velocity were at noise level; the fine screens and contraction damped out the disturbance caused by the toaster and coarse screen). However, when the grid was placed in the flow, very smooth mean profiles were generated (see §3.1). The test-section speed for these toaster experiments was 6·3 m/s.

Velocity fluctuations were measured with DISA type-55M constant-temperature bridges. The u (longitudinal velocity) and w (lateral velocity) components were measured with a 90° X-wire array with length-to-diameter ratio l/d of 200 and overheat ratio of 1·8. The wires were 3·2 μm tungsten. Simultaneous temperature fluctuations were measured with a 1·27 μm platinum wire ($l/d = 400$) placed close to the X-array. The fast-response a.c. temperature bridge was the same as that used by Warhaft & Lumley (1978). Measurements of temperature fluctuations in a 'cold' flow revealed that the r.m.s. noise level (combined electrical and tunnel) was approximately 5×10^{-3} °C. Temperature-fluctuation measurements were corrected for noise and velocity contamination and the effect of finite wire length was accounted for in the X-wire measurements. The mean temperature profiles were measured with a chromel–constantan thermocouple with a reference temperature maintained by a compensation unit. All data acquisition and analysis was done on a PDP 11/34 minicomputer. Further experimental details may be found in Sirivat (1983).

3. The results

First we shall present the salient characteristics of the velocity field and then we shall examine the transverse homogeneity of the thermal variance and heat flux. Finally the results of the evolution of the temperature variance, heat flux and related length- and timescale ratios for both the mandoline and toaster experiments will be presented.

3.1. *The velocity field*

Figure 4 shows the decay rate for $\overline{u^2}$ and $\overline{w^2}$, the longitudinal and transverse mean-square velocity fluctuations, for the two different speeds studied: 3·4 m/s ($Re_M = 5150$) and 6·3 m/s ($Re_M = 9545$). The normalized decay laws deduced from these data, as well as other parameters, are listed in table 1. Note (figure 4 and table 1) that u/w is always greater than unity; at $x/M = 100$, for example, it is approximately 1·06. Thus there is slight anisotropy in the velocity field, as is usually observed in grid turbulence (Comte-Bellot & Corrsin 1966). Figure 5 shows the turbulence-energy dissipation rate ϵ ($\equiv \nu \overline{u_{ij}, u_{ij}}$) determined using 3 different methods: differentiation of the energy decay law ($\epsilon = -\frac{1}{2}d\overline{q^2}/dt$, where $\overline{q^2} = \overline{u^2} + 2\overline{w^2}$), integration of the velocity spectrum ($\epsilon = 7{\cdot}5\nu \int_0^\infty k^2 \phi_w(k)\, dk$, where $\phi_w(k)$ is the one-dimensional w-spectrum and k is wavenumber), and from the velocity derivative

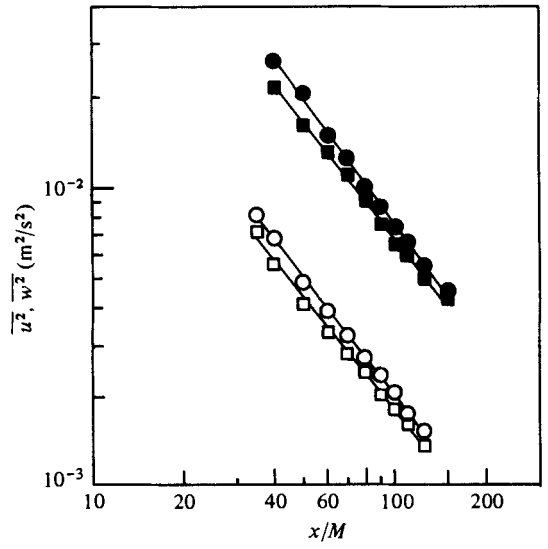

FIGURE 4. The decay of the longitudinal variance $\overline{u^2}$ and cross-stream variance $\overline{w^2}$: ●, ■, $\overline{u^2}$ and $\overline{w^2}$ for $U = 6{\cdot}3$ m/s; ○, □, $\overline{u^2}$ and $\overline{w^2}$ for $U = 3{\cdot}4$ m/s. See also table 1.

		$U = 3{\cdot}4$ m/s	$U = 6{\cdot}3$ m/s
M (m)		0·025	0·025
$\overline{u^2}/U^2 = A(x/M)^{-n}$	n	1·29	1·37
	A	0·0664	0·1051
$\overline{w^2}/U^2 = A(x/M)^{-n}$	n	1·24	1·29
	A	0·0468	0·062
r.m.s. u (m/s)		$4{\cdot}49 \times 10^{-2}$	$8{\cdot}71 \times 10^{-2}$
r.m.s. w (m/s)		$4{\cdot}23 \times 10^{-2}$	$8{\cdot}06 \times 10^{-2}$
$\epsilon = -\frac{3}{2}(d\overline{u^2}/dt)$ (m^2/s^3)		$5{\cdot}31 \times 10^{-3}$	$3{\cdot}93 \times 10^{-2}$
$l = (\overline{u^2})^{\frac{3}{2}}/\epsilon$ (m)		$1{\cdot}71 \times 10^{-2}$	$1{\cdot}68 \times 10^{-2}$
$\lambda_g = (15\nu\overline{u^2}/\epsilon)^{\frac{1}{2}}$ (m)		$9{\cdot}70 \times 10^{-3}$	$6{\cdot}91 \times 10^{-3}$
$\eta = (\nu^3/\epsilon)^{\frac{1}{4}}$ (m)		$9{\cdot}59 \times 10^{-4}$	$5{\cdot}82 \times 10^{-4}$
$Re_M = UM/\nu$		5150	9545
$Re_l = ul/\nu$		46·5	88·9
$Re_\lambda = u\lambda_g/\nu$		26·4	36·5
$\tau_u = 3\overline{u^2}/\epsilon$ (s)		1·14	0·58

TABLE 1. Velocity flow parameters. The fluctuation parameters are calculated for $x/M = 100$. $\nu = 1{\cdot}65 \times 10^{-5}$ m^2/s.

($\epsilon = 15\nu\overline{(du/dx)^2}$). The good agreement among the three methods shows that using the assumption of isotropy for the velocity field, as is done for the integral and derivative methods, yields results close to the third method in which ϵ is calculated directly from the rate of decay of the turbulence energy. Thus the assumption of isotropy is not a bad one.

Figure 6 shows the evolution of the longitudinal integral lengthscale L. L was obtained by evaluating the autocorrelation function of u and integrating up to its first zero and then using the Taylor 'frozen' assumption to convert time to length: $L = UT$, where U is the mean velocity and T is the integral of the autocorrelation function. There is indeed a large amount of scatter in these measurements, approx-

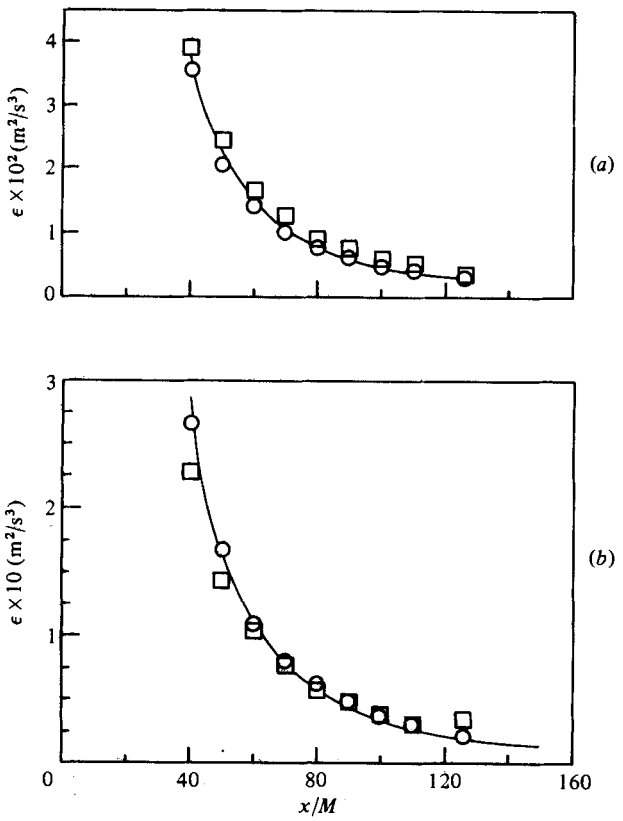

FIGURE 5. The decay of the turbulence-energy dissipation rate ϵ. ○, $\epsilon = 15\nu\overline{(du/dx)^2}$; □, $\epsilon = 7{\cdot}5\nu \int_0^\infty k^2\phi_w(k)\,dk$; solid line, $\epsilon = -\frac{1}{2}d\overline{q^2}/dt$. (*a*) $U = 3{\cdot}4$ m/s; (*b*) $U = 6{\cdot}3$ m/s.

imately $\pm 7\,\%$ about the fitted line to the data. This is approximately the same scatter observed by Sreenivasan *et al.* (1980), which is marked on the figure. As was done by these workers, we will use a fitted line to these data when, in §3.3, we compare values of the velocity integral scale with those of the thermal integral scale.

3.2. *The cross-stream thermal characteristics*

Figure 7 shows the cross-stream mean temperature for the mandoline (2, 1) (the notation 'mandoline (x, y)' means that the mandoline is placed x mesh lengths from the grid with y mesh lengths spacing between the wires). As with the previous workers (Wiskind 1962; Alexopoulos & Keffer 1971; Venkataramani & Chevray 1978) we achieved linear temperature gradients. Other gradients and mandoline configurations used ((2, 2) and (10, 1)) produced equally pleasing results. Figure 8 shows the cross-stream r.m.s. temperature profiles for the two mean profiles of figure 7. The scatter across the core of the flow (which is approximately 8 mesh lengths) is typically 5 % deviation about the mean once the flow has developed ($x/M \approx 40$). These profiles should be compared and contrasted with the profiles of the previous workers (who used heated grids), which are shown in figure 2. For the case $\beta = 7{\cdot}48$ °C/m we have also drawn the transverse r.m.s. θ profile for $x/M = 15$, i.e. for the region close to the grid. Here we see the effect of the differentially heated mandoline wires: there is a very strong gradient in r.m.s. θ across the core of the flow since the hotter wires produce higher r.m.s. However, by $x/M = 40$ a homogeneous profile is established.

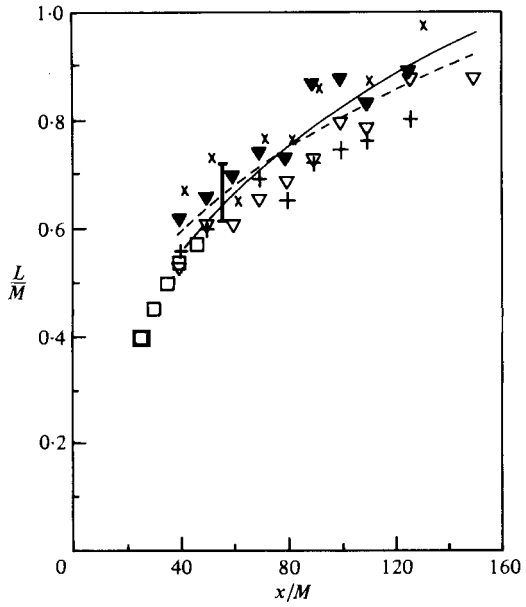

FIGURE 6. Evolution of the longitudinal velocity lengthscale L derived from the longitudinal autocorrelation function. ×, ▼, $U = 3{\cdot}4$ m/s; ▽, +, $U = 6{\cdot}3$ m/s (two different experiments for each speed). ---, best fit to the data; ——, Sreenivasan *et al.* (1980); □, Yeh & Van Atta (1973). The vertical bar indicates the scatter of the measurements of Sreenivasan *et al.* (1980).

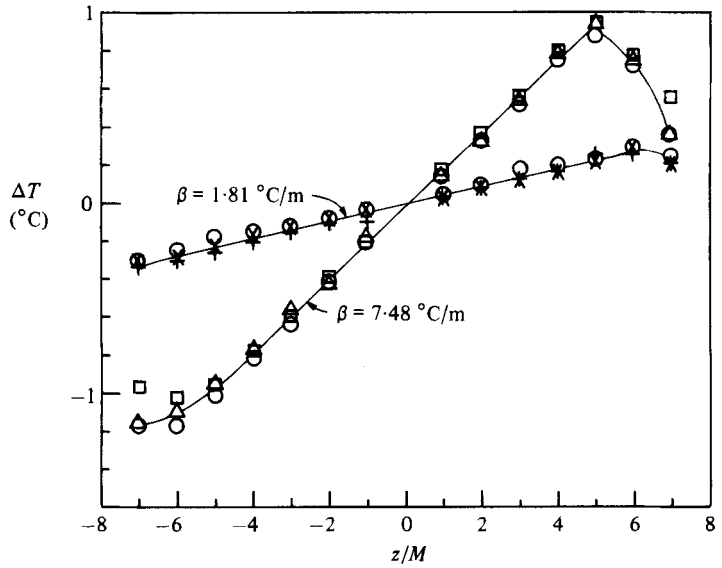

FIGURE 7. Some mean cross-stream temperature profiles for the mandoline (2, 1), $U = 3{\cdot}4$ m/s. (*a*) $\beta = 1{\cdot}81$ °C/m: ○, $x/M = 45$; +, 75; ×, 115. (*b*) $\beta = 7{\cdot}48$ °C/m: □, $x/M = 45$; △, 65; ○, 115.

For the heated grid experiments good homogeneity is never attained (figure 2). This may be in part due to the strong coherence between u and θ that occurs in heated-grid experiments. The cross-correlation coefficient $\rho_{u\theta}$, between u and θ for heated-grid experiments has been found to be as high as $-0{\cdot}3$ (Warhaft & Lumley 1978); ideally it should be zero. For the mandoline experiments $\rho_{u\theta}$ is typically $-0{\cdot}05$.

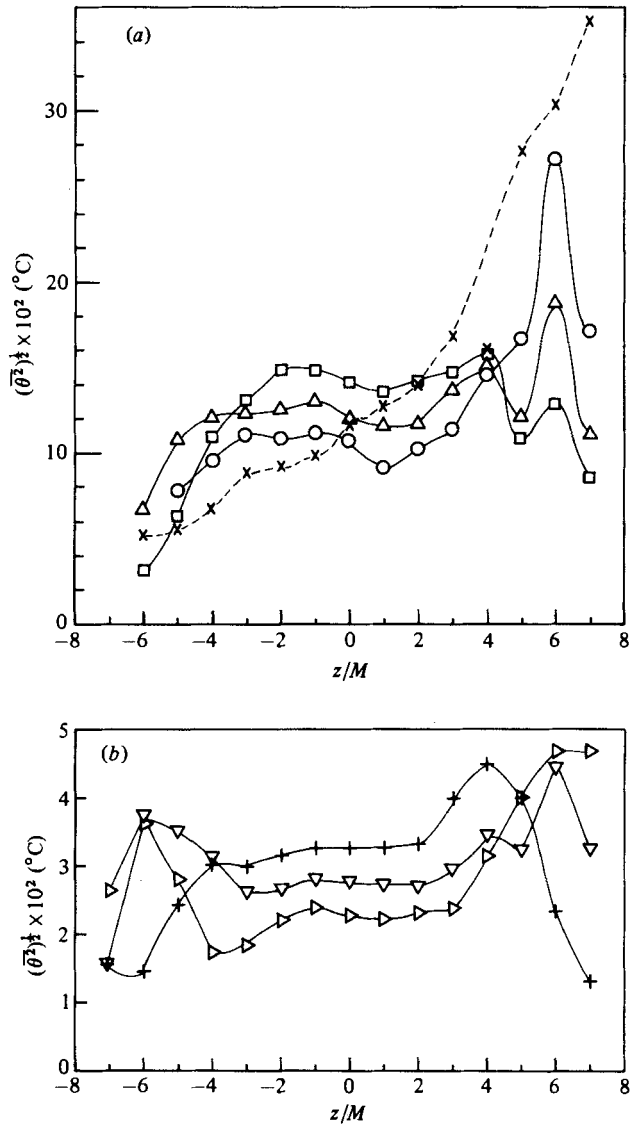

FIGURE 8. Transverse (cross-stream) r.m.s. θ-homogeneity for the mandoline (2, 1). (*a*) $\beta = 7{\cdot}48$ °C/m, $U = 3{\cdot}4$ m/s: ×, $x/M = 15$; ○, 40; △, 80; □, 110. (*b*) $\beta = 1{\cdot}81$ °C/m, $U = 3{\cdot}4$ m/s: ▷, $x/M = 50$; ▽, 90; +, 126.

Figure 9 shows the mean cross-stream temperature gradient for the toaster; as for the mandoline experiments a high degree of linearity was achieved. The example shown in figure 9 is for $\beta = 10{\cdot}3$ °C/m, other gradients examined (10·0 °C/m and 3·68 °C/m) gave the same degree of linearity. Figure 10 shows the transverse r.m.s. θ for the toaster experiment. While there is some initial inhomogeneity, after $x/m \approx 100$ there is only $\pm 3\,\%$ variation of r.m.s. θ across the core of the flow, which is about 7 mesh lengths wide.

Figure 11 shows the transverse profiles of $\overline{\theta w}$, $\overline{\theta^2 w}$ and ϵ_θ (see §3.3 for the method of determining ϵ_θ) for mandoline (2, 1), $\beta = 7{\cdot}48$ °C/m. Apart from the good homogeneity of $\overline{\theta w}$ and ϵ_θ, figure 11 gives the rationale for neglecting the third-moment

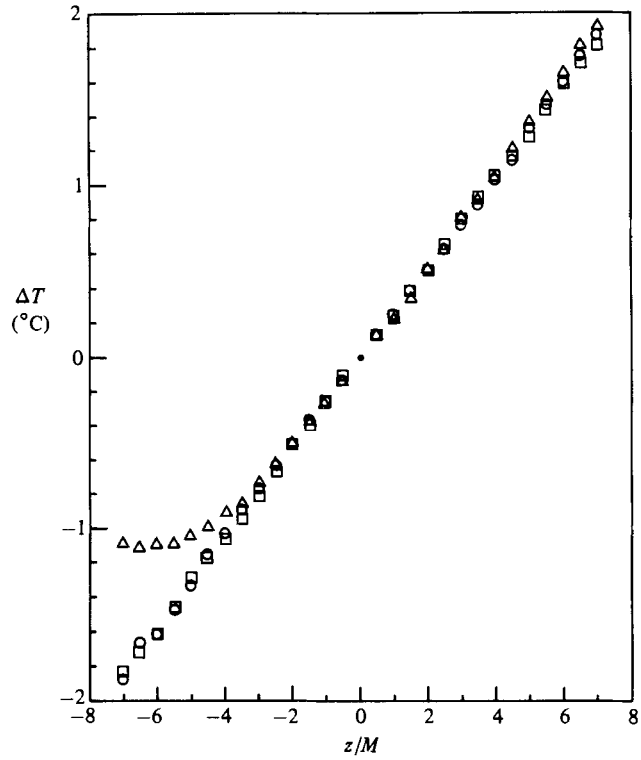

FIGURE 9. A mean cross-stream temperature profile for the toaster, $U = 6{\cdot}3$ m/s: □, $x/M = 65$; ○, 115; △, 155.

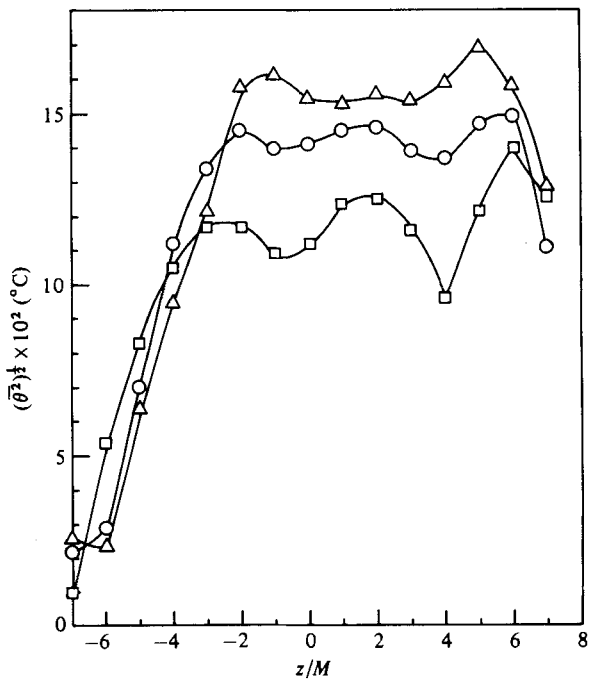

FIGURE 10. Transverse r.m.s. θ-homogeneity for the toaster, $U = 6{\cdot}3$ m/s, $\beta = 10{\cdot}3$ °C/m: □, $x/M = 60$; ○, 110; △, 150.

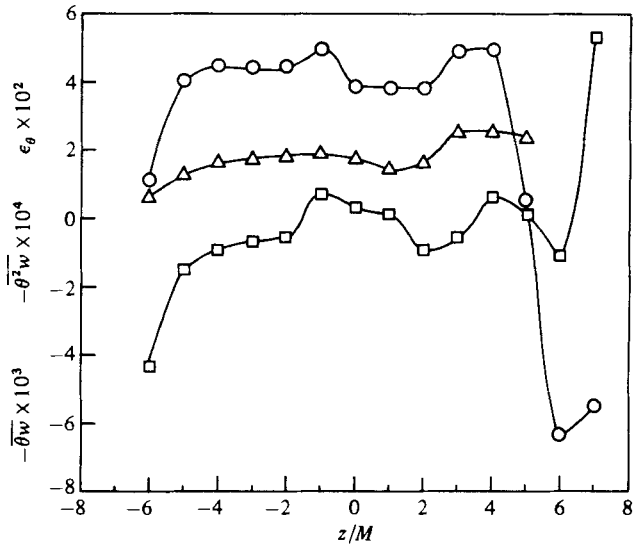

FIGURE 11. Transverse homogeneity of second- and third-order quantities for the mandoline, $U = 3{\cdot}4$ m/s, $\beta = 7{\cdot}48$ °C/m: ○, $\overline{\theta w}$ (°Cm/s); △, ϵ_θ (°C²/s); □, $\overline{\theta^2 w}$ (°C² m/s).

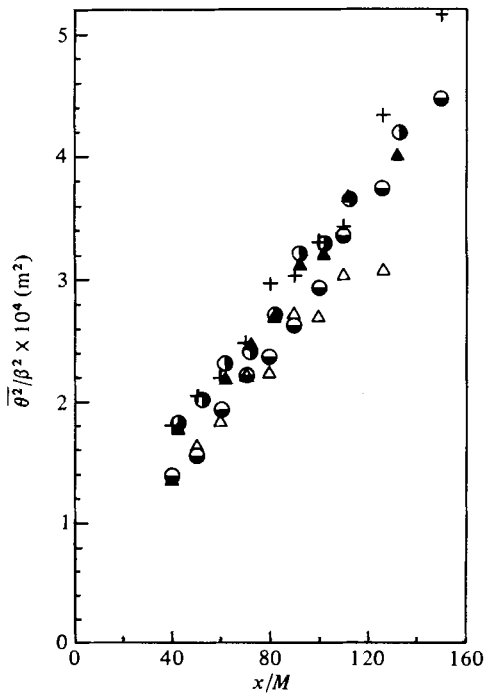

FIGURE 12. $\overline{\theta^2}/\beta^2$ for mandoline (2, 1), $U = 3{\cdot}4$ m/s: ◒, $\beta = 8{\cdot}1$ °C/m; +, 7·48 °C/m; ◑, 6·4 °C/m; ▲, 4·3 °C/m; △, 1·81 °C/m. See also table 2.

term $(\frac{1}{2}d\overline{\theta^2 w}/dz)$ in the $\overline{\theta^2}$ budget. The highest possible value for this term that can be obtained from figure 11 is only a few per cent of the production term or rate term in (1) (see §3.3 for the values of these quantities). The molecular smearing term in the $\overline{\theta w}$ budget has been neglected for the same reason; it is negligible compared with the other terms in (2) (Sirivat 1983).

Mandoline configuration	Mandoline wire diameter (mm)	β (°C/m)	$A \times 10^5$ (m²)	$\frac{1}{2\beta^2}\frac{d\overline{\theta^2}}{dt} \times 10^4$ (m²/s)	$\frac{\overline{\theta^2}}{\beta^2} \times 10^4$ (m²)	$K_\theta \times 10^4$ (m²/s)
(2, 1)	0·203	1·81	5·95	1·44	2·68	4·89
(2, 1)	0·127	4·3	6·10	1·79	3·20	—
(2, 1)	0·127	6·4	5·40	1·89	3·3	—
(2, 1)	0·127	7·48	8·01	1·67	3·31	5·09
(2, 1)	0·203	8·1	1·89	1·92	2·94	5·39
(2, 2)	0·203	1·78	—	0·89	1·54	3·16
(10, 1)	0·203	2·24	—	1·02	2·04	4·33

TABLE 2. Some temperature-field parameters for the mandoline experiments. $U = 3{\cdot}4$ m/s for all cases. A, the y-axis intercept (figure 12) was determined by a line of best fit to the data. The variance gradient (column 5) was also determined from a line of best fit. (For the case $\beta = 7{\cdot}48$ °C/m the last two values (figure 12) were neglected.) The last three columns were determined for $x/M = 100$.

3.3. *Evolution of the thermal field*

3.3.1. *The mandoline experiments.* Figure 12 shows, for the mandoline (2, 1), $\overline{\theta^2}/\beta^2$ *vs.* x/M for 5 different values of β (varying from 1·81 °C/m to 8·1 °C/m), and table 2 summarizes the salient characteristics of the data. Although there is some scatter, a straight line produces the best fit to the data. We have normalized the temperature variance by β^2, and this produces a reasonable collapse of the data. Note that (1) can be written in the form

$$\frac{1}{2\beta^2}\frac{d\overline{\theta^2}}{dt} = K_\theta - \frac{\epsilon_\theta}{\beta^2}. \tag{3}$$

Below we shall report the production and dissipation terms in the form of (3) since these data, for various β, also collapse well using this normalization. The origin (figure 12) is at $x/M \approx -20$; shifting this origin to zero does not appreciably change the form of the trend in the data. Figure 13 shows $\overline{\theta^2}/\beta^2$ for two further mandoline configurations, (2, 2) and (10, 1), and these are contrasted with one of the (2, 1) cases. The dashed lines indicate that the thermal field was inhomogeneous. Note that for (2, 2) and (10, 1) the temperature variance first decreases, and then it increases as production begins to dominate dissipation. This also occurred for the (2, 1) cases (figure 12), but for these cases by $x/M = 40$ production was more dominant than dissipation (we did not plot these early points (in the initially inhomogeneous flow) on the graphs of figure 12). Of course in all these experiments, there must be an initial $\overline{\theta^2}$ since we are introducing the temperature gradient by means of heating wires which also produce temperature fluctuations. Furthermore, by changing the initial mandoline configurations, we are changing the initial thermal to velocity lengthscale ratio (Warhaft & Lumley 1978).†

Insight into the evolution of $\overline{\theta^2}$ in figure 13 may be gained by examining the

† We note that mandoline (2, 1) produces the lengthscale ratio closest to unity (see figure 14). (2, 2) produces a slightly smaller thermal scale than (2, 1), a result contrary to expectation, which would suggest that a larger wire spacing should produce a larger scale (as always occurs when the mandoline is placed further downstream; (10, 1) produces a smaller scale than (10, 2) for example). The anomalous behaviour when the thermal field is introduced very close to the grid (the same anomaly occurs for helium – Sirivat & Warhaft 1982) is probably due to the complex interaction of the thermal field with the strongly anisotropic velocity wake. Nevertheless (for $\beta = 0$) the positive correlation between faster decay rate and smaller input scale (Warhaft & Lumley 1978) is still maintained no matter where (or how) the scalar is introduced. Thus (2, 2) has a higher decay rate than (2, 1) when $\beta = 0$ (Sirivat 1983).

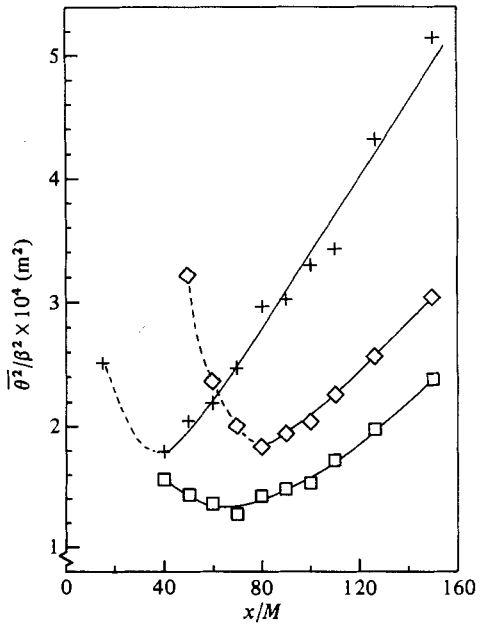

FIGURE 13. $\overline{\theta^2}/\beta$ for different mandoline configurations: +, mandoline (2, 1), $\beta = 7{\cdot}48$ °C/m (from figure 12), □, (2, 2), 1·78 °C/m; ◇, (10, 1), 2·24 °C/m. $U = 3{\cdot}4$ m/s in all cases. The dashed line indicates that the thermal variance had not yet reached homogeneity in the transverse direction.

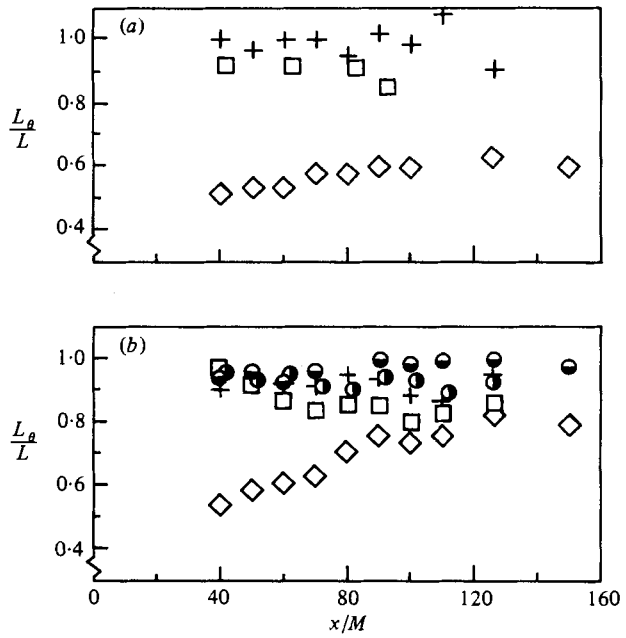

FIGURE 14. Thermal/mechanical longitudinal lengthscale ratio L_θ/L for the mandoline experiments. (*a*) No-gradient case ($\beta = 0$): +, mandoline (2, 1); □, (2, 2); ◇, (10, 1). (*b*) Gradient cases: +, mandoline (2, 1), $\beta = 7{\cdot}48$ °C/m; ◔, (2, 1), 6·4 °C/m; ◒, (2, 1), 8·1 °C/m; □, (2, 2), 1·78 °C/m; ◇, (10, 1), 2·24 °C/m. $U = 3{\cdot}4$ m/s in all cases.

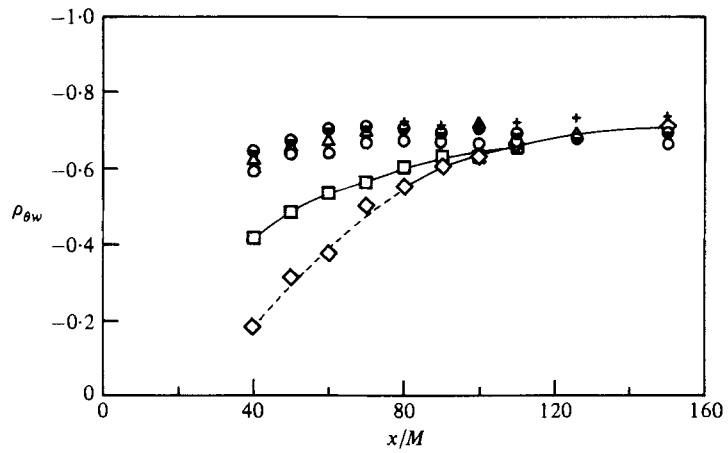

FIGURE 15. $\rho_{\theta w}$ for the mandoline experiments. ◒, △, +: β = 8·1, 1·81, 7·48 °C/m respectively, mandoline (2, 1), U = 3·4 m/s. ○, mandoline (2, 1), β = 4·48 °C/m, U = 6·3 m/s; □, (2, 2), 1·78 °C/m, 3·4 m/s; ◇, (10, 1), 2·24 °C/m, 3·4 m/s.

evolution of the thermal and mechanical lengthscales. Figure 14(*a*) shows L_θ/L, the ratio of the longitudinal thermal to velocity integral scales (deduced from the autocorrelation functions) for the cases in which $\beta = 0$ (i.e. decaying temperature variance). For mandoline (2, 1) $L_\theta/L \approx 1$, but for (10, 1) this ratio is initially 0·5. As the flow evolves for this non-gradient case the lengthscale ratio remains approximately constant (as was previously found by Warhaft & Lumley 1978). However, when the temperature gradient is imposed on the flow (figure 14*b*) the lengthscale ratio for the case (10, 1) is driven up to the equilibrium value for the case (2, 1). This value is approximately 0·9, although there is large scatter. It is quite clear, however, that, while in the absence of production (decaying $\overline{\theta^2}$) the lengthscale ratio remains (approximately) at its initial value, with production present there is a trend to an equilibrium lengthscale ratio.† This value appears to be around 0·9 (figure 14*b*). Thus the thermal gradient forces the lengthscale ratio to a constant value, regardless of its initial value, which is determined by the mandoline configuration. When this value has been achieved, the production dominates the dissipation in the temperature variance budget and the increase in $\overline{\theta^2}/\beta^2$ is approximately linear (figure 13).

Figure 15 shows the evolution of the cross-correlation $\rho_{\theta w}$ between θ and w, where w is the velocity fluctuation in the direction of β. Here too we see that if there is a mismatch in the initial L_θ/L (mandolines (2, 2) and (10, 1), figure 14) the magnitude of $\rho_{\theta w}$ grows until it reaches a constant value of −0·7, while if the initial value of L_θ/L is approximately unity (mandoline (2, 1), figure 14) then $\rho_{\theta w}$ remains approximately constant. The equilibrium value $\rho_{\theta w} = -0{\cdot}7$ should be compared with the lower values of −0·48 and −0·6 reported by Wiskind (1962) and Venkataramani & Chevray (1978) respectively. However, as mentioned above, their flows had significant transverse inhomogeneity. Furthermore, the plot of $\overline{\theta^2}$ (figure 1) for their two experiments suggests that the thermal field was still evolving, and thus $\rho_{\theta w}$ may not have reached its equilibrium value. It will be shown below that the toaster, an entirely

† There is, in fact, a slight increase in the lengthscale ratio for the mandoline (10, 1), for the case without the temperature gradient (figure 14*a*). However, this increase is far less pronounced than for the case where the gradient is present (figure 14*b*). Sreenivasan *et al.* (1980) also find a gradual increase in L_θ/L for their (zero-temperature-gradient) heated-screen experiments in which the initial scalar scale was much smaller than the velocity scale.

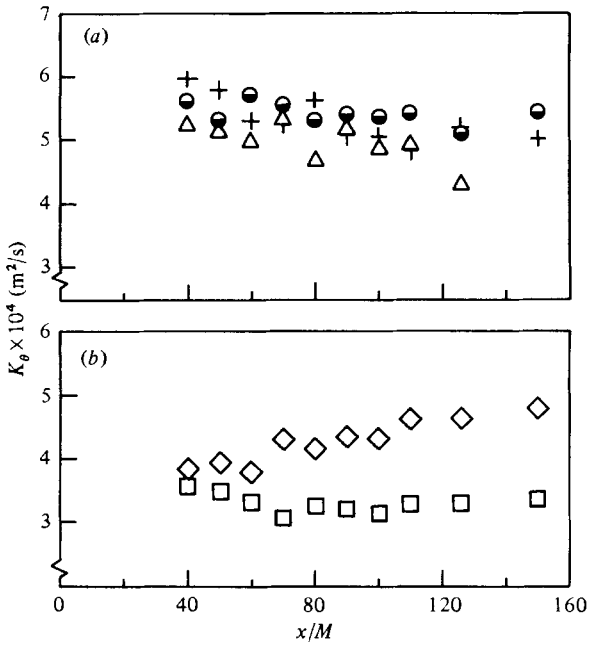

FIGURE 16. (*a*) Thermal eddy diffusivity for mandoline (2, 1). (*b*) Thermal eddy diffusivity for mandoline (10, 1) (◇) and mandoline (2, 2) (□). The symbols are the same as for figure 15.

different method of generating the temperature gradient, also produced a value of $\rho_{\theta w} \approx -0{\cdot}7$.

Figure 16 shows the evolution of K_θ ($\equiv -\overline{\theta w}/\beta$), the thermal eddy diffusivity. For the mandoline (2, 1) (figure 16*a*) its value decreases slowly with x/M, showing that the gradient-production term (2) does not quite keep pace with the return-to-isotropy term. Of course we would expect K_θ to decrease since the Reynolds number of the flow is slowly decreasing. In §1 it was shown that the turbulence Re is proportional to t^{1-n}, where $n = 1{\cdot}29$ (table 1); the value of K_θ (figure 16*a*) is diminishing at approximately this rate. We note also that the value of K_θ at $x/M = 100$ is approximately 5×10^{-4} m²/s; thus the ratio K_θ/κ, where κ is the thermal diffusivity, is 22, and this is comparable to the value of the turbulence Re ($\equiv ul/v$), which is 46·5 at this position. For the mandolines (2, 2) and (10, 1) the initial value of K_θ is lower than for (2, 1) (figure 16*b*), as would be expected since $\rho_{\theta w}$ is initially weak (figure 15), but after L_θ/L achieves its equilibrium value at about $x/M = 80$ there is a gradual increase in K_θ for these two cases.

Figure 17 shows the temperature-variance dissipation rate for the various mandoline experiments, determined by subtracting the production term from the rate term in (1). For the mandoline (2, 1) (figure 17*a*) ϵ_θ/β^2 decreases at approximately the same rate as K_θ (figure 16*a*), but for the cases where the scalar is introduced at a significantly different lengthscale to the velocity lengthscale (mandolines (2, 2) and (10, 1)) the initial dissipation rate is higher (figure 17*b*), as is suggested by figure 13, but it rapidly decreases as the lengthscale ratio tends to its equilibrium value (figure 14*b*). Figure 18 compares ϵ_θ computed by means of the differencing method with ϵ_θ computed using two methods that make the assumption of local isotropy. The three methods compare reasonably well (fitted curves would be within about 10 % of each other), indicating that, although the large-scale thermal field is anisotropic (because

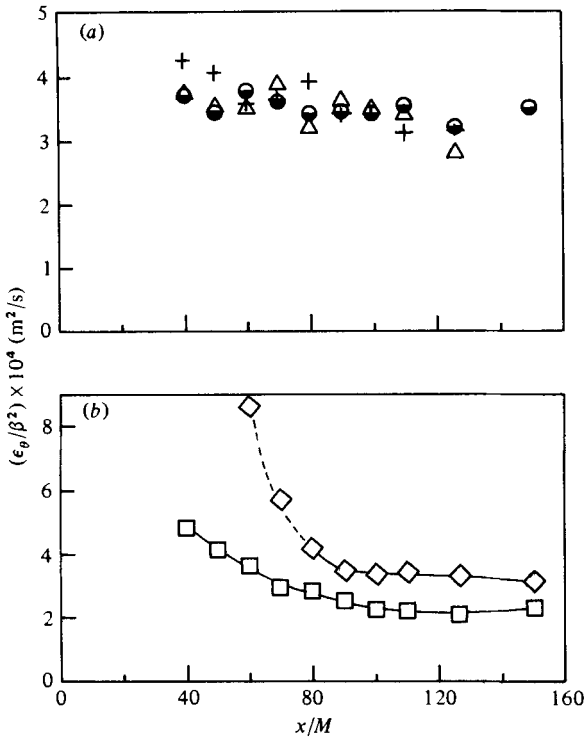

FIGURE 17. ϵ_θ/β^2 for the mandoline experiments: (*a*) mandoline (2, 1), same symbols as figure 16(*a*); (*b*) mandolines (2, 2) and (10, 1), same symbols as figure 16(*b*). ϵ_θ has been determined from the difference between the rate term and the production term (equation (1)).

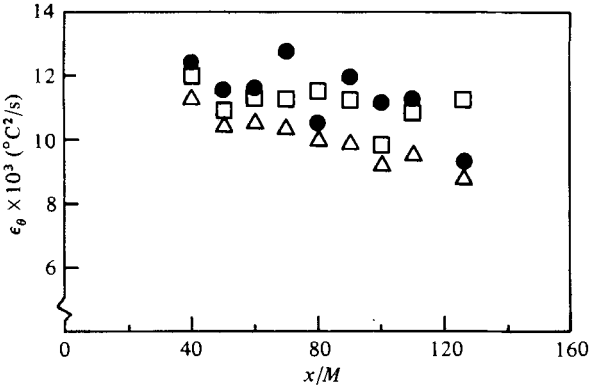

FIGURE 18. ϵ_θ determined by 3 different methods: △, $\epsilon_\theta = 3\kappa\,\overline{(d\theta/dx)^2}$; □, $\epsilon_\theta = 3\kappa \int_0^\infty k^2 \phi_\theta(k)\,dk$; ●, ϵ_θ determined from difference between rate term and production term (equation (1)). For all cases $\beta = 1{\cdot}81$ °C/m, $U = 3{\cdot}4$ m/s mandoline (2, 1).

of the thermal gradient), the assumption of small-scale isotropy is still valid for this flow. It should be noted that this assumption cannot be generally made for the small-scale thermal field. For example, for flows with a mean velocity gradient as well as a mean temperature gradient, pronounced skewness of the temperature derivative is observed (Sreenivasan & Tavoularis 1980). In our experiments, the magnitude of the skewness of the temperature derivative was small ($< 0{\cdot}15$).

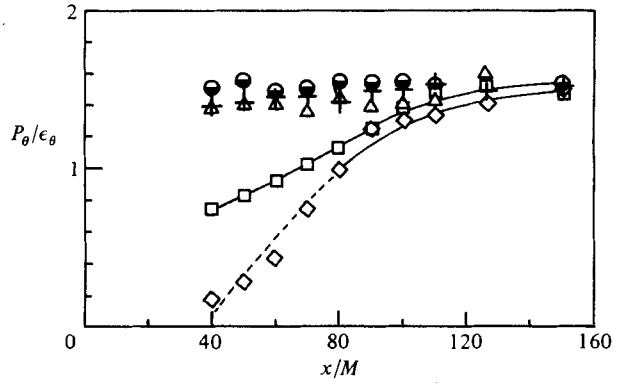

FIGURE 19. The ratio of temperature variance production P_θ to variance dissipation ϵ_θ for the mandoline experiments. Symbols are the same as figure 15.

In decaying grid turbulence with a mean temperature gradient there are three timescales: the velocity timescale τ ($\equiv \overline{q^2}/\epsilon$), the dissipation timescale of the thermal field $\tau_{\theta 1}$ ($\equiv \overline{\theta^2}/\epsilon_\theta$) and the production timescale of the thermal field $\tau_{\theta 2}$ ($\equiv \overline{\theta^2}/-\overline{\theta w}\beta$). Figure 19 shows the thermal dissipation to thermal production timescale ratio $\tau_{\theta 1}/\tau_{\theta 2}$ ($= P_\theta/\epsilon_\theta$, where $P_\theta \equiv -\overline{\theta w}\beta$) for all the mandoline experiments. For the mandoline (2, 1), the situation in which the scalar is introduced at its approximate equilibrium lengthscale (figure 14), P_θ/ϵ_θ has an approximately constant value of about 1·5 for all values of β; varying β not only reduces the production, it also reduces dissipation proportionately, maintaining this timescale ratio at 1·5. For mandolines (2, 2) and (10, 1), P_θ/ϵ_θ is initially less than unity, i.e. dissipation is initially more dominant than production (as is evident from figure 13), but, for these cases also, the ratio rises to a value of approximately 1·5 as equilibrium is attained.

Another relevant timescale ratio is the mechanical dissipation to thermal dissipation ratio $(\overline{q^2}/\epsilon)/(\overline{\theta^2}/\epsilon_\theta)$, which is usually denoted by r (Warhaft & Lumley 1978). For decaying temperature fluctuations in grid turbulence $r = m/n$, where n and m are the respective exponents of the power-law decays for velocity and temperature variance. Figure 20 shows r calculated for the gradient experiments. For the mandoline (2, 1) $r \approx 1{\cdot}3$, although there is significant scatter between the various gradient cases (compare this with the timescale ratio P_θ/ϵ_θ (figure 19), where there is only about 5% scatter for the mandoline (2, 1) cases). We note that, unlike the case of decaying temperature variance where $r = m/n$, here the value of r ($= (2/n)t/(\overline{\theta^2}/\epsilon_\theta)$, where t is real time from the grid) is critically dependent on absolute values of variance, and the scatter in figure 20 undoubtedly reflects cumulative calibration and measurement error rather than any trend. For the mandolines (2, 2) and (10, 1), figure 20 shows that, as for the lengthscale ratio (figure 14*b*) and as for the ratio P_θ/ϵ_θ (figure 19), the gradient also drives r toward an equilibrium value if there is a mismatch in the initial thermal and velocity scales, although because of scatter, and also because r for (2, 2) and r for (10, 1) have probably not yet reached their final value (r at $x/M = 150$ still appears to be decreasing for these two cases), its precise equilibrium value cannot be determined from figure 20; it appears to be $1{\cdot}4 \pm 0{\cdot}2$.

The above experiments were carried out for three different mandoline configurations only ((2, 1), (2, 2) and (10, 1)). An attempt was made to do a further experiment with the mandoline at (20, 1), but the r.m.s. θ remained inhomogeneous in the cross-stream direction for the full extent of the tunnel. This was probably due to the inability of

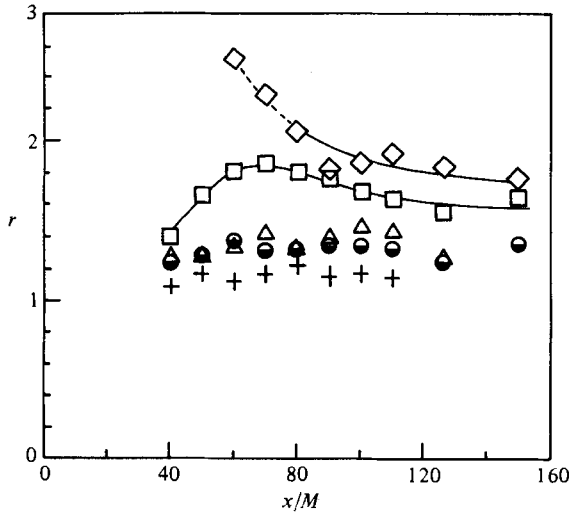

FIGURE 20. The mechanical/thermal timescale ratio r for the mandoline experiments. Symbols are the same as figure 15.

the reduced turbulence intensity (at $x/M = 20$) to mix the initially inhomogeneous temperature variance produced by the differentially heated mandoline wires when they were placed this far downstream from the grid. (We note for the experiments where the mandoline was placed at $x/M = 2$ a homogeneous transverse r.m.s. θ-profile was achieved by about $x/M = 40$, but for the mandoline at $x/M = 10$ it took until about $x/M = 80$ to achieve a flat transverse r.m.s. θ-profile.) However the way in which such parameters as the thermal length- and timescales (figures 14, 19 and 20) and $\rho_{\theta w}$ (figure 15) asymptote towards equilibrium values for the above three different mandoline configurations suggests that if the temperature gradient and temperature fluctuations could, in some way, have been established with an initial thermal lengthscale even smaller than that achieved with the mandoline at (10, 1), the same equilibrium values for these parameters would have resulted, although their initial values would have been further from equilibrium than for the case (10, 1). Thus we believe we have observed the essential features of the evolution of the thermal characteristics for this type of flow. It is also worth noting that although the mandoline was placed in the region of the flow in which the grid-bar wakes were still coalescing (homogeneity of the velocity field does not occur until about 15–20 mesh length from the grid), this did not appear to affect the nature of the fine-scale thermal field. By the downstream position where the measurements commence ($x/M = 40$) the skewness of the temperature derivative as well as the temperature–longitudinal-velocity cross-correlation coefficient were negligible, indicating that the thermal field was not affected by the large-scale structures of the grid bars (as was the case for heated-grid flows – Warhaft & Lumley 1978).

3.3.2. *The toaster experiments.* Figure 21 shows the evolution of $\overline{\theta^2}/\beta^2$ for 3 toaster experiments for which $\beta = 10{\cdot}3$ °C/m, 10·0 °C/m and 3·68 °C/m, and table 3 lists some of the data parameters. The mean speed was 6·3 m/s for these experiments. In order to compare these results with those of the mandoline (done at 3·4 m/s) we have used time ($= x/U$, where U is the mean velocity) for the abscissa. The dashed line is the average value of the measurements of figure 12 (mandoline (2, 1), $U = 3{\cdot}4$ m/s). Also included in the figure is a case for the mandoline (2, 1), but with $U = 6{\cdot}3$ m/s, the

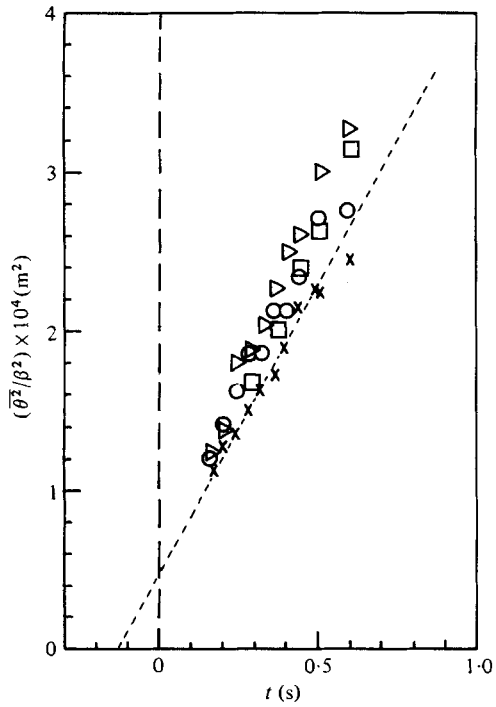

FIGURE 21. $\overline{\theta^2}/\beta^2$ for the toaster experiments and for a further mandoline experiment; $U = 6{\cdot}3$ m/s in all cases: ○, toaster, $\beta = 10{\cdot}3$ °C/m; □, toaster, 10·0 °C/m; ▷, toaster, 3·68 °C/m; ×, mandoline (2, 1), 4·48 °C/m. See also table 3. Dashed line is the average of the mandoline (2, 1) experiments, $U = 3{\cdot}4$ m/s (figure 12).

	β (°C/m)	$A \times 10^5$ (m^2)	$\frac{1}{2\beta^2}\frac{d\overline{\theta^2}}{dt} \times 10^4$ (m^2/s)	$\frac{\overline{\theta^2}}{\beta^2} \times 10^4$ (m^2)	$K_\theta \times 10^4$ (m^2/s)
Toaster	3·68	5·62	2·37	2·45	8·97
Toaster	10·0	3·86	2·30	2·21	—
Toaster	10·3	7·39	1·83	2·19	7·84
Mandoline (2, 1)	4·48	6·93	1·47	1·90	7·46

TABLE 3. Some temperature-field parameters for the toaster experiments. $U = 6{\cdot}3$ m/s for all cases. Also included is a mandoline (2, 1) experiment done at the same speed (6·3 m/s). The last 3 columns were evaluated for $x/M = 100$ ($t = 0{\cdot}397$ s). A, the y-axis intercept (figure 21) was determined from a line of best fit to each data set.

same speed as for the toaster experiments. The variance produced by the toaster also increases at an approximately linear rate, which is slightly greater than that for the mandoline (2, 1).

Figure 22 shows the lengthscale ratio L_θ/L for the toaster experiments and for the mandoline (2, 1), $U = 6{\cdot}3$ m/s. The equilibrium value is about 0·85, i.e. about the same value as for the mandoline experiments (figure 14*b*). Of course for the toaster experiments we were unable to alter the initial value of L_θ/L since in these experiments the thermal lengthscale is produced solely by the turbulent mixing against the thermal gradient. As for the mandoline experiments the equilibrium value

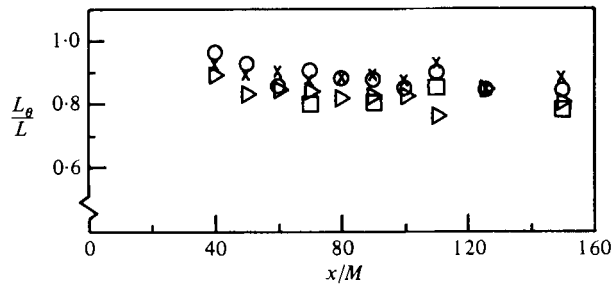

FIGURE 22. L_θ/L for the toaster experiments, $U = 6{\cdot}3$ m/s, and for mandoline (2, 1), $U = 6{\cdot}3$ m/s. Symbols are the same as for figure 21.

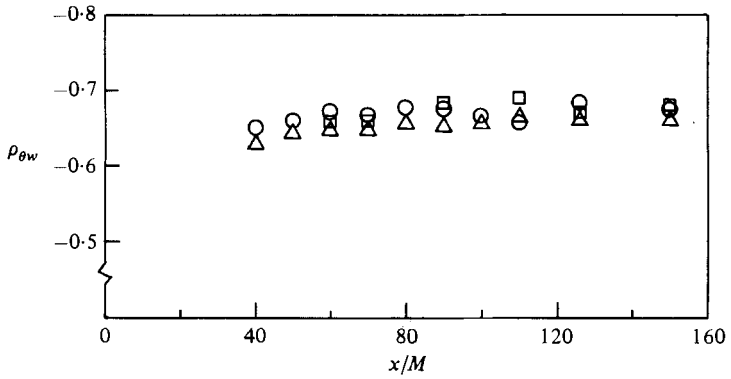

FIGURE 23. $\epsilon_{\theta w}$ for the toaster experiments, $U = 6{\cdot}3$ m/s: ○, $\beta = 10{\cdot}3$ °C/m; □, 10·0 °C/m; △, 3·68 °C/m.

of L_θ/L is independent of β. The cross-correlation $\rho_{\theta w}$ between θ and w is shown in figure 23. Its equilibrium value of approximately $-0{\cdot}68$ is close to that of the mandoline experiments (figure 15).

Figure 24 shows the eddy diffusivity and thermal dissipation rate for the toaster and for the mandoline (2, 1), $U = 6{\cdot}3$ m/s. These values should be compared with those of the mandoline (2, 1), slow speed (figures 16*a*, 17*a*). For the fast speed (figure 24) both K_θ and ϵ_θ/β^2 have increased, reflecting the higher turbulence Reynolds number (table 1). They also tend to decrease at a slightly faster rate than for the slow-speed case. The reason for this, and for the slightly faster rate of increase of $\overline{\theta^2}/\beta^2$ (figure 21) is not clear.

Finally we present the timescale ratios for the toaster experiments (figure 25). P_θ/ϵ_θ (figure 25*a*) has a value of 1·4 at $x/M = 150$, a value in good agreement with that of the equilibrium value of 1·5 for the mandoline experiments (figure 19). We note that, at $x/M = 150$, P_θ/ϵ_θ is still gradually increasing for the toaster experiment. This may be due to the higher speed used in this experiment; because the speed was nearly twice that used for the mandoline experiments, by $x/M = 150$ the elapsed time is only half that of the slow-speed mandoline experiments and the field may not yet be at its equilibrium value. r for the toaster (and for the mandoline (2, 1), $U = 6{\cdot}3$ m/s) is shown in figure 25(*b*). As for the slow-speed mandoline cases (figure 20), there is fairly large scatter. The average value appears to be $1{\cdot}6 \pm 0{\cdot}2$; slightly higher than r for the slow-speed mandoline experiments.

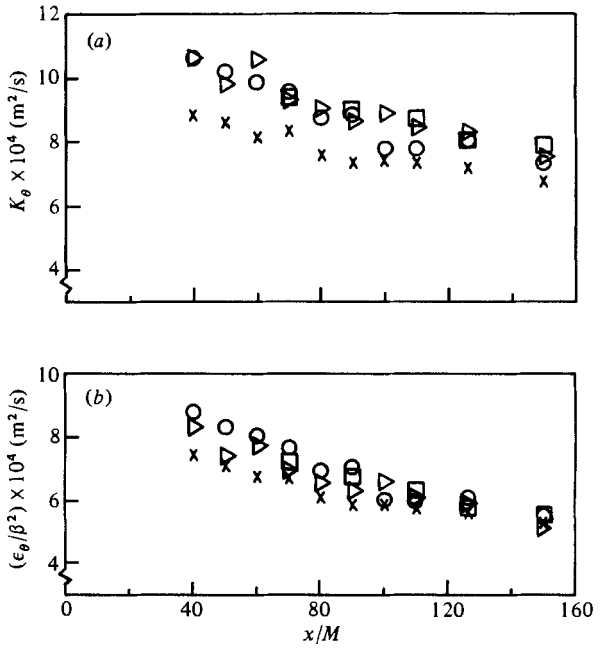

FIGURE 24. (a) Eddy diffusivity K_θ and (b) temperature-variance dissipation rate ϵ_θ/β^2 for the same experiments as figure 21. Symbols are the same as for figure 21.

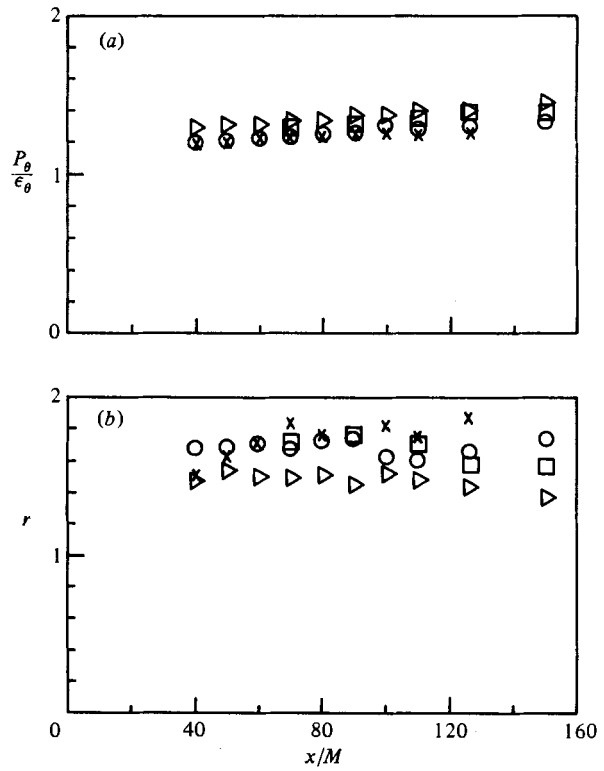

FIGURE 25. (a) The ratio of temperature-variance production P_θ to temperature-variance dissipation ϵ_θ, and (b) the mechanical/thermal timescale ratio r for the same experiments as figure 21. Symbols are the same as for figure 21.

4. Conclusions

We have described two new methods for producing a linear temperature gradient in decaying grid-generated turbulence. Both methods produced good transverse homogeneity in the thermal field, in contrast with the experiments of previous workers using heated grids. For the mandoline experiments we have shown that the temperature gradient forces the lengthscale ratio L_θ/L and the timescale ratios $(\overline{\theta^2}/\epsilon_\theta)/(\overline{\theta^2}/P_\theta)$ and $(\overline{q^2}/\epsilon)/(\overline{\theta^2}/\epsilon_\theta)$ to equilibrate to constant values; values that are independent of the magnitude of the gradient β. The variation of initial magnitudes of these ratios was effected by varying the mandoline configuration. Once the equilibrium length- and timescale ratios had been established the temperature variance grew linearly with time.

For the toaster, which produces a temperature gradient, but for which the temperature variance is produced solely by the action of turbulence production against this gradient (in contrast with the mandoline, whose wires produce an initial temperature variance as well as a gradient), the values of length- and timescale ratios were similar to those of the equilibrium values produced by the mandoline, and the temperature variance also grew linearly with time, although at a slightly higher rate than for the mandoline.

The equilibrium values for the ratio of the thermal/mechanical lengthscale and thermal variance production/dissipation are approximately 0·9 and 1·5 respectively for all the experiments reported here, regardless of how the gradient was produced. The equilibrium value for the mechanical/thermal timescale ratio r is less certain; although there is a tendency for it to equilibrate there is considerable scatter in the data for this quantity. It appears to be approximately 1·4 for the mandoline experiments, but slightly higher (about 1·6) for the toaster experiments, although for the latter case the field may not have reached final equilibrium because of the shorter elapsed time (faster speed) of this experiment.

The above results should be contrasted with the thermal-variance evolution in decaying grid turbulence without gradient production (Warhaft & Lumley 1978). In that case the thermal/mechanical lengthscale ratio did not change with time and there was no equilibrium value for the thermal-variance decay rate. We note that in a previous experiment (Warhaft 1980) we attempted to force L_θ/L to an equilibrium value by applying mean strain to the field, but this had the effect of driving the system further from equilibrium.

We thank Professor J. L. Lumley for discussions and Mr E. P. Jordan for his continued excellent technical assistance. This work was funded by grants from the Engineering Section and Atmospheric Section of the U.S. National Science Foundation. The respective grant numbers are MEA-8104733 and ATM 7922006.

REFERENCES

ALEXOPOULOS, C. C. & KEFFER, J. F. 1971 Turbulent wake in a passively stratified field. *Phys. Fluids* **14**, 216–224.

COMTE-BELLOT, G. & CORRSIN, S. 1966 The use of a contraction to improve the isotropy of grid-generated turbulence. *J. Fluid Mech.* **25**, 257–682.

CORRSIN, S. 1952 Heat transfer in isotropic turbulence. *J. Appl. Phys.* **23**, 113–118.

DURBIN, P. A. 1980 A stochastic model of two-particle dispersion and concentration fluctuations in homogeneous turbulence. *J. Fluid Mech.* **100**, 279–302.

SIRIVAT, A. 1983 Thesis, Sibley School of Mechanical and Aerospace Engineering, Cornell University.

SIRIVAT, A. & WARHAFT, Z. 1982 The mixing of passive helium and temperature fluctuations in grid turbulence. *J. Fluid Mech.* **120**, 475–504.

SREENIVASAN, K. R. & TAVOULARIS, S. 1980 On the skewness of the temperature derivative in turbulent flows. *J. Fluid Mech.* **101**, 783–795.

SREENIVASAN, K. R., TAVOULARIS, S., HENRY, R. & CORRSIN, S. 1980 Temperature fluctuations and scales in grid-generated turbulence. *J. Fluid Mech.* **100**, 597–622.

SULLIVAN, P. J. 1976 Dispersion of line source in grid turbulence. *Phys. Fluids* **19**, 159–161.

TENNEKES, H. & LUMLEY, J. L. 1972 *A First Course in Turbulence.* MIT Press.

VENKATARAMANI, K. S. & CHEVRAY, R. 1978 Statistical features of heat transfer in grid generated turbulence – constant-gradient case. *J. Fluid Mech.* **86**, 513–543.

WARHAFT, Z. 1980 An experimental study of the effect of uniform strain on thermal fluctuations in grid-generated turbulence. *J. Fluid Mech.* **99**, 545–573.

WARHAFT, Z. & LUMLEY, J. L. 1978 An experimental study of the decay of temperature fluctuations in grid-generated turbulence. *J. Fluid Mech.* **88**, 659–684.

WISKIND, H. K. 1962 A uniform gradient turbulent transport experiment. *J. Geophys. Res.* **67**, 3033–3048.

YEH, T. T. & VAN ATTA, C. W. 1973 Spectral transfer of scalar and velocity fields in heated-grid turbulence. *J. Fluid Mech.* **58**, 233–261.